Paper ThP.IV-10

HIF 2000

Development of the 2-MV Injector for HIF*

F. M. Bieniosek, J. W. Kwan, E. Henestroza, C. Kim

Lawrence Berkeley National Laboratory

Berkeley, CA 94720

Abstract

The 2-MV Injector consists of a 17-cm-diameter surface ionization source, an extraction diode, and an electrostatic quadrupole (ESQ) accelerator, with maximum current of 0.8 A of potassium beam at 2 MeV. Previous performance of the Injector produced a beam with adequate current and emittance but with a hollow profile at the end of the ESQ section. We have examined the profile of the beam as it leaves the diode. The measured nonuniform beam density distribution qualitatively agrees with EGUN simulation. Implications for emittance growth in the post acceleration and transport phase will be investigated.

PACS Codes: 29.27.Ac, 41.75.Ak

Keywords: Heavy Ion Fusion, Injector, Pulsed Power

Corresponding Author:

Frank Bieniosek
LBNL
MS 47-112
1 Cyclotron Rd.
Berkeley CA 94720 USA

Tel: 510-486-5456
Fax: 510-486-7392
Email: fmbieniosek@lbl.gov

1. Introduction

A typical heavy-ion fusion driver has 84 beam channels with each channel transporting a beam of line charge density 0.25 _C/m. A 2 MV electrostatic quadrupole (ESQ) injector [1-4], representing a single driver beam, has been in operation at Lawrence Berkeley National Laboratory for several years. The initial goal of the 2-MV Injector project was to demonstrate the feasibility of an injector that has the required energy, current, and emittance of the injector for a full-scale fusion driver. This goal was achieved relatively early in the project. Recent work on the Injector has had the goals of studying the behavior of the beam in the source and diode regions, improving the reliability of the equipment, and preparing the 2-MV Injector for its future role as the injector for the High Current Experiment (HCX).

The 2-MV Injector is contained inside a pressure vessel which houses the 38-stage Marx generator, the 2-MV dome containing the ion source and electronics, and the electrostatic quadrupole (ESQ) transport and accelerating section. The pressure vessel provides electrical insulation of the high voltage structure and is typically pressurized to 5 atmospheres of CO_2. Each stage of the Marx generator consists of a simple network of parallel LC and RC circuits arranged to produce a $4-\mu s$ flattop voltage flat to within 0.5%. The slope of the output voltage pulse can be adjusted by changing the conductivity of a load water resistor. At present the source is a 17-cm diameter spherically curved hot porous tungsten contact ionizer source emitting Cs^+ ions. The source is normally negatively biased at up to –80 kV with respect to the extractor electrode, which is at dome potential, to inhibit ion emission from the hot surface. Beam extraction is performed during a portion of the Marx generator flattop by pulsing the source voltage positive with respect to the dome using a pulse forming network (PFN) coupled to the source through a step-up transformer.

Previous performance of the Injector produced a beam with adequate current and emittance but with a hollow intensity profile at the end of the ESQ section [2,4]. Results using a K^+ aluminosilicate ion source have indicated that beams at the design level of 0.8 A at 2 MeV were produced with normalized edge emittance of less than 1 π mm-mrad. However beam profile measurements at the end of the ESQ section

showed clear evidence of beam hollowing, rippling and halos. On the other hand, beam profile measurements at other axial locations in the structure showed profiles that were not hollow. Evolutionary behavior of this sort is not inconsistent with theoretical predictions. For example, a numerical simulation (Fig. 5 of Ref. [5]) shows the typical evolution of an initially parabolic beam density distribution at the diode exit. The distribution evolves into a sharply hollow distribution after the second ESQ (Q2), and later returns to a uniform distribution at the fourth ESQ (Q4). Several evolutions were calculated in Ref [5]. Interestingly, they tend to show little emittance growth over a limited transport distance. The results of these investigations suggest that a nonuniform beam distribution forms in the diode region of the Injector.

2. Initial results

Figure 1 shows the Injector accelerating column, including the source, extraction electrode, and ESQ column. We installed a multiple Faraday cup array (FCA) to examine the beam optics at the diode. It consists of an array of small Faraday cups (1-mm diameter entrance aperture) arranged in two orthogonal rows mounted in a single movable assembly. The collectors are staggered in radius with a center to center separation of 3.8 mm, beginning at 1.9 mm in the nominally horizontal direction, and at 3.8 mm in the nominally vertical direction. Note that there is no collector in the array precisely on axis. The assembly can be rotated and moved along the beam axis inside the ESQ column. The FCA was mounted on a stalk and inserted through the center of the ESQ column (from the right side of Figure 1), to study the evolution of beam profiles at and downstream of the end of the diode section. Figure 2 shows the configuration of the collectors on the FCA. Not shown is a cylindrical suppressor electrode in front of the FCA, typically biased at –10 kV, whose purpose is to prevent secondary electrons created on the face of the collector array from entering the diode region. The profile measured at the end of the ESQ was hollow, as previously determined. Kapton and Mylar films were inserted at this location and they also showed a hollow beam profile, consistent with the FCA data.

To study beam behavior in the diode region, the Injector was reconfigured. The ESQ section, and the final 28 of the 38 stages of the 2-MV Marx generator, were shorted out for these tests. The maximum diode

accelerating voltage, equivalent to 2.0 MV in the complete device, is 750 kV. Two types of ion sources were using in this investigation: a K^+ aluminosilicate source, and K^+ or Cs^+ contact ionizer source. The aluminosilicate source was prepared by melting a thin layer of aluminosilicate loaded with potassium to form a smooth coating on the porous tungsten substrate of the source [6]. The contact ionizer source was prepared by applying a water-based solution of K_2CO_3 or Cs_2CO_3 on the bare porous tungsten substrate [7]. Baking at a temperature in excess of 500°C dissociates the carbonate, and releases CO and CO_2.

Three types of waveforms (Figure 3) are observed on the FCA. The data presented in Figure 3 are typical data, taken with the cesium contact ionizer source and with the collectors reverse biased to collect secondary electrons to enhance signal strength. The signals observed on the collectors not at the center or edge of the beam are typically flat during the beam pulse, consistent with the expected flat beam current pulse. The central horizontal collector (at 1.9 mm) has a signal strongly growing with time during the pulse; the central vertical collector (at 3.8 mm) may also show some time variation. The collector nearest to the edge of the beam typically exhibits some degree of rippling in the collected current waveform. Figure 4 is a comparison between mid-pulse profiles obtained using a K^+ aluminosilicate source, and a K^+ contact ionizer source. In both cases the beam profile at the exit of the diode is sharply peaked on axis. The profile for the aluminosilicate source is a vertical scan, and the profile for the contact ionizer is a horizontal scan. The collectors were biased with respect to the grid electrode to suppress secondary electrons. The vacuum pressure in this case, measured at the downstream end of the Injector, was 2×10^{-6} Torr, corresponding to an estimated pressure of $3\text{-}5 \times 10^{-5}$ Torr near the source.

3. Discussion of initial results

The peaked current distribution of Figure 3 is inconsistent with the beam distribution in the diode predicted from simulation. Several possible causes for the observed behavior have been investigated.

(a) Insufficient or nonuniform beam emission from the surface of the source. In order to study the uniformity of emission we have made a comparison of measurements between two types of ion

sources: an aluminosilicate source, and a porous tungsten contact ionizer source (Figure 3). Mobility of the dopant ion on the hot surface of the ionizer is sufficiently high that, given a reasonably uniform temperature profile across the face of the source, uniformity of emission is not expected to be an issue with a contact ionizer. The source temperature under operating conditions is nearly uniform: typically 960°C in the center of the face of the source, and 940°C on the outer edge of the source. The current density requirement for space-charge-limited extraction (5 mA/cm^2 for potassium) should be easily achievable for both types of ion source at this temperature.

(b) Poor vacuum conditions, leading to significant modification of space charge and beam loss due to charge-exchange and ionization on the residual gas. Local pressure at the source can be high because of poor conductance to the vacuum pumps, which are necessarily located away from the diode near the downstream end of the ESQ section. As the beam ions are accelerated in the diode, they may interact with the residual gas in the region, as well as with Cs or K neutrals emitted from the source itself. The predominant residual gas species during operation are CO, CO_2, H_2O and H_2. Given that cross sections for charge exchange [7] are typically in the range of 2×10^{-16} cm^2, at an ambient pressure in the diode region of 5×10^{-5} Torr, the fraction of beam ions undergoing charge exchange is on the order of 1%. Charge-exchange neutrals created in interaction between the beam and residual gas or Cs neutrals will be geometrically focused in the diode because of the converging shape of the source, to provide a peak in signal at the center of the detector array. The energetic neutrals could appear as charged particles if they are stripped by gas evolved at the entrance aperture to the detector.

To minimize any effect of residual gases on beam transport in the diode, we have redesigned the source to eliminate a vacuum leak, instituted a bake-out procedure, and installed a cold cathode gauge to monitor the pressure at the ion source. Typical operating pressure at the ion source has been reduced by more than an order of magnitude, to about 1×10^{-6} Torr.

(c) Incorrect geometry or incorrect voltages on the diode electrodes. Geometry of the ion gun has been carefully checked against the design configuration, and the voltage on the extraction electrode, which is the electrode most crucial to operation of the diode, shows no sign of loading during the beam pulse.

A sensitivity study for the diode region was performed using the EGUN code [9,10]. This study reviewed the Injector design work done at the time of the initial assembly of the Injector. The nominal beam profiles along the surface of the source and at the exit of the diode are approximately uniform, with a radius of 2.7 cm at the collector array. Effects of various emission deficiencies, voltage variations, and geometric deformations on the beam profile and other beam parameters were studied. Among the possibilities considered, some combination of emission deficiencies were studied as potential candidates. Several cases of imperfect emission were investigated. In the case of source emission that is uniform but below the Child-Langmuir limit, the radius of the beam rapidly collapses near the gun exit. If emission at the source is hollow, the lack of repulsive space charge forces in the middle of the beam cause the beam to implode toward the axis. On the other hand if the source emission is concentrated near the center, the beam comes out of the gun more divergent.

The width of the beam profile at the diode exit of the gun is controlled by the ratio between the extraction and accelerating voltages, which has been verified by experiment. Geometric distortions of the gun electrodes, including voltages on the gradient rings and spherical and translation deformations in the range of ±1 mm also have an effect on the beam profiles, but it is less pronounced than the effects described previously. Installation of the large Faraday cup, as noted below, will allow more detailed quantitative comparisons between the model and the experiment.

4. Recent results

The K^+ contact ionizer source exhibited a short lifetime, probably associated with a high neutral fraction, leading to rapid loss of the ions stored in the source substrate. The ratio of ion to neutral flux in a contact ionizer is determined by the Saha-Langmuir equation

$$\frac{\nu_i}{\nu_n} = 2\exp\left(\frac{\phi - I}{kT}\right)$$

where ϕ is the work function of the metal and I is the ionization potential of the adsorbed atom. Given that the ionization potential is 4.34 eV for potassium, and 3.89 eV for cesium, the ratio of ions to neutrals for a clean tungsten surface (ϕ =4.55 eV) is about 25 for potassium and over 5000 for cesium. The presence of adsorbed atoms lowers the work function, further reducing the ion-to-neutral ratio. Thus the neutral fraction, and the loss rate of adsorbed atoms, is expected to be much higher for a K^+ source than for a Cs^+ source, because the loss of adsorbed atoms is predominantly due to the continuous neutral flux between beam pulses. In order to operate with a source lifetime long enough to adequately bake the vacuum system, we have performed most of our measurements with a Cs contact ionizer source.

The extractor pulse length was extended from less than 2 μs to 3 μs for Cs operation. This is necessary because of the long time of flight of the cesium beam through the diode. The longer beam pulse more closely resembles the longer pulse lengths (7 to 20 _s) desired in the HCX. The Marx generator pulse will also have to be lengthened for the HCX, because it is too short to accommodate the transit of the beam through the entire ESQ structure.

Figure 5 shows a vertical profile of a 460-keV Cs^+ beam at the collector array at t = 1.5 μs. The pressure measured near the source was 1.3 x 10^{-6} Torr. The time of flight of the beam from the source to the face of the collector array is 1 μs. Thus taking into account the rise time of the beam pulse, this data represents the beam profile at the beginning of the 'flat top' phase of the beam pulse. The central peak is strongly localized on axis, and increases in amplitude during the beam pulse, but the beam current in the central peak remains <10% of the total intercepted beam. The peak appears predominantly on the radially innermost collector, which is located at a distance of 1.9 mm from the axis of the diode. The amplitude of the central peak is affected by the suppressor voltage in the 10 kV range, and it grows less rapidly further downstream from the diode, suggesting that it consists of medium energy particles, or is an artifact of the

measurement. The body of the pulse also exhibits time and spatial variation during the beam pulse flattop to a lesser degree.

Figure 6 shows an EGUN simulation of the profile of the beam at the diode plate. It has characteristics similar to the data of Figure 5, in particular the presence of 'ears' at the outer edge of the profile and the central peak. The ears in the simulation are caused by geometric aberration in the diode, and may be eliminated by modifying the design.

5. Conclusions.

Investigation of the shape and time behavior of the ion beam in the diode region indicates that the beam is already nonuniform as it leaves the diode. The profile is peaked both at the center and at the edge. The amplitude of the central peak appears to be affected by the quality of the vacuum in the diode. It may represent lower energy charged particles, not the heavy ion beam. The presence of this distribution of ions is likely to perturb the space charge in the diode, leading to distortions in the bulk of the beam. The beam nonuniformity is not due to emission variations on the surface of the source, or alignment of the electrode geometry. The nonuniform beam density distribution early in the beam pulse qualitatively agrees with EGUN simulation. An estimate of emittance growth due to the nonlinear electrostatic field energy [10,11] of the density distribution exiting the diode (Figure 6) indicates that the contribution from nonlinear field energy is significantly larger than the other contributing effects considered, thermal emittance of the source and nonlinearities in the optics. As a result it is important to understand and control the beam profile.

6. Future plans

Investigation of the nonuniform beam profile will continue. We plan to monitor the evolution of the measured profile as the surface concentration of cesium on the source substrate varies, and use electric or magnetic deflecting fields to determine the energy and charge components of the central peak. We are planning to improve the FCA diagnostic to reduce its sensitivity to local beam-plasma effects at the

collector surface. We are installing a large Faraday cup to measure the total beam current exiting the diode for direct comparison with the space-charge-limit current. Source electrical current measurements show current drain comparable to the space-charge limit current, but these measurements could include a component of backstreaming electron current.

The large-format source as demonstrated on the 2-MV Injector is a low current-density option for HIF injectors. Our present plan is to upgrade the Injector for high-current beam transport experiments while other compact source options are explored.

- We plan to increase the Marx generator pulse length to 7 μs. The increased pulse length will be achieved by first increasing the value of the water resistor utilized to grade the voltages on the diode stack and ESQ focusing elements, and second increasing the inductance of the Marx generator tray circuits from 300 μH to 600 μH. The increased pulse length will provide increased opportunity to study long-pulse effects over pulse lengths representative of a fusion driver.
- Potassium ion beams are preferred for the HCX because of their higher velocity and higher beam current than equivalent Cs^+ beams. Therefore we are developing a new K^+ aluminosilicate source for the 2-MV Injector. The source consists of a sintered aluminosilicate – molybdenum graded mixture with a smooth transition between a molybdenum base layer to an aluminosilicate-rich surface layer. The smooth transition provides a large reservoir of active aluminosilicate material at the surface while eliminating any tendency toward separation between the aluminosilicate and the substrate metal [12].

7. Acknowledgements.

The authors gratefully acknowledge the advice and encouragement of Andy Faltens, and the technical assistance of our support staff, including Ralph Hipple, Tak Katayanagi, David Beck, Bill Strelo and Jerry Stoker.

References.

[1] L. Reginato, C. Peters, Engineering research and development for the Elise heavy ion induction accelerator, Fusion Engineering and Design 32-33 (1996) 337-345.

[2] S.S. Yu, et.al., 2 MV Injector as the Elise front-end and as an experimental facility, Fusion Engineering and Design 32-33 (1996) 309-315.

[3] W. Abraham, et.al., Design and testing of the 2 MV Heavy Ion Injector for the fusion energy research program, Proc. 1995 Particle Accelerator Conference, Paper WPA01.

[4] S. Yu, et.al., Heavy ion fusion 2 MV Injector, Proc 1995 Particle Accelerator Conference, Paper TAE01.

[5] S.M. Lund, et.al., Numerical simulation of intense-beam experiments at LLNL and LBNL, Nuclear Instruments and Methods A415 (1998) 34-356.

[6] J.W. Kwan, Ion sources for heavy ion fusion induction linacs, Nuclear Instruments and Methods A415 (1998) 268-273.

[7] S MacLaren, et.al., A high-current density contact ionization source for heavy-ion fusion, Proc. 1999 Particle Accelerator Conference, p. 2849.

[8] H.H. Lo and W.L. Fite, Atomic Data 1, 305-328 (1970).

[9] W.B. Hermannsfeldt, Electron trajectory program, SLAC Report 226 (1979).

[10] C. Kim, A sensitivity study for the K^+ gun of the 2 MeV Injector, LBNL Internal Report HIFAN 976, LBNL 43688 (Dec. 15, 1998).

[11] T.P. Wangler, K.R Crandall, R.S. Mills, and M. Reiser, Relation between field energy and RMS emittance in intense particle beams, IEEE Trans. On Nuclear Science, NS-32, 2196 (1985).

[12] D.W. Hughes, R.K. Feeney, and D.N. Hill, Aluminosilicate-composite type ion source of alkali ions, Rev. Sci. Instrum. 51 (1980) p 1471-2.

*Work supported by DOE, Office of Fusion Science, under DOE Contract No. DE-AC03-76F00098.

Figure Captions.

Figure 1. Extraction diode and ESQ sections of the 2-MV heavy-ion Injector.

Figure 2. The Faraday cup array (FCA) diagnostic.

Figure 3. Typical FCA data with Cs^+ beam, showing three types of waveforms. The central collector has a signal growing with time during the pulse. The majority of the pulses are flat during the beam pulse ("typical collector"). Finally, some of the edge collectors show ripples ("edge ripples"). Time is referenced to the leading edge of the extractor voltage pulse.

Figure 4. Profiles of the beam current collected at the FCA for a contact ionizer source and an aluminosilicate source with a relatively high vacuum pressure at the ionization gauge of about 2 x 10-6 Torr. The collector array is located in its full forward position. In this position, the front face of the collector is 19 cm downstream of the diode plate.

Figure 5. Horizontal profile of a 460-keV Cs^+ beam at t = 1.5 μs at 19 cm downstream, biased to collect secondary electrons, and scaled to estimated beam current density by assuming a secondary multiplication coefficient of 26. Markers indicate the collector locations.

Figure 6. EGUN calculation of a 460-keV Cs^+ beam current density profile at the diode plate.

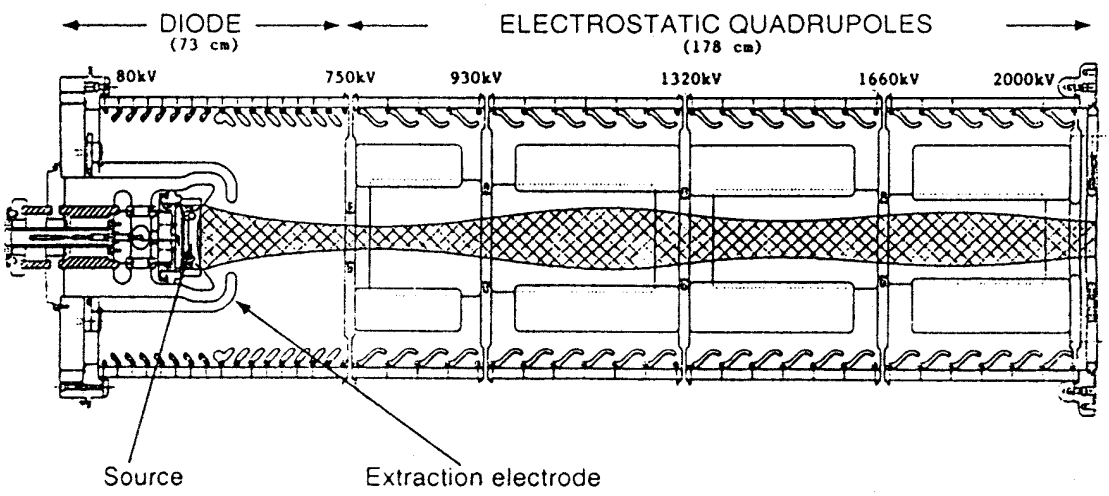
DIODE
(73 cm)
ELECTROSTATIC QUADRUPOLES
(178 cm)
80kV
750kV
930kV
1320kV
1660kV
2000kV
Source
Extraction electrode

Figure 1.

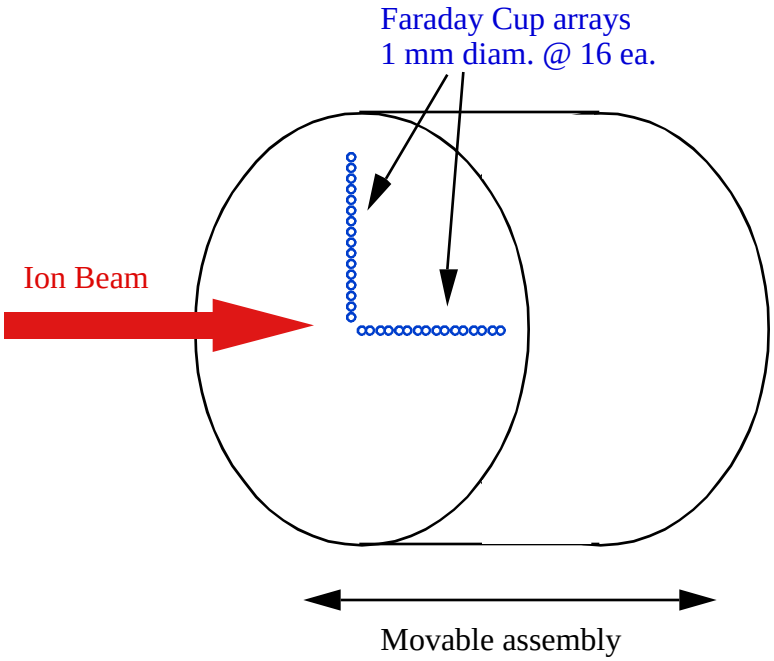

Figure 2.

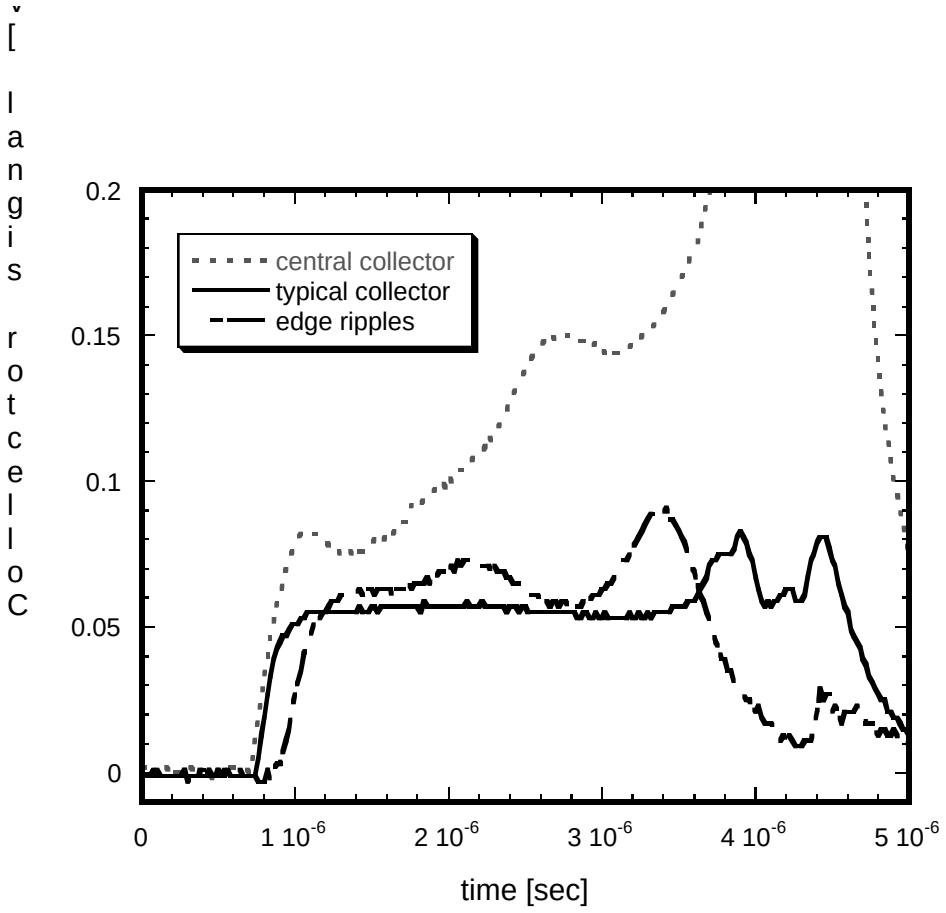
Collector current [A]
0.2
0.15
0.1
0.05
0
central collector
typical collector
edge ripples
0
1 10-6
2 10-6
3 10-6
4 10-6
5 10-6
time [sec]

Figure 3.

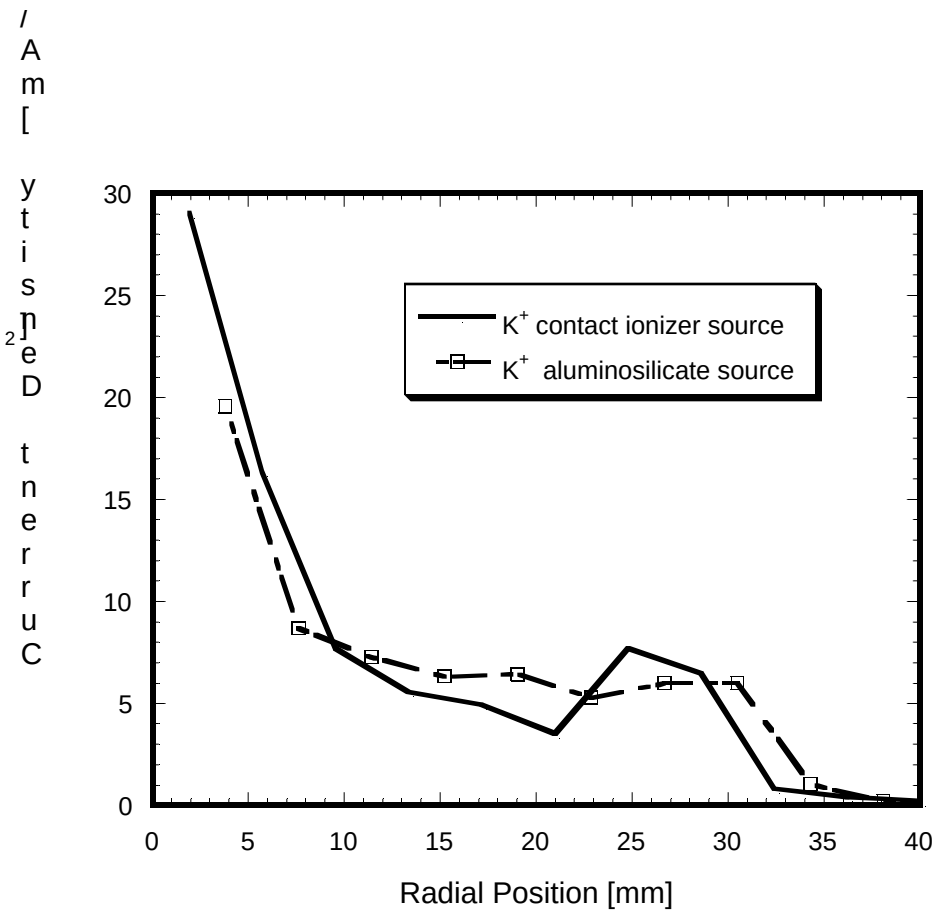
Current Density [mA/cm2]
30
25
20
15
10
5
0
0
5
10
15
20
25
30
35
40
Radial Position [mm]
K+ contact ionizer source
K+ aluminosilicate source

Figure 4.

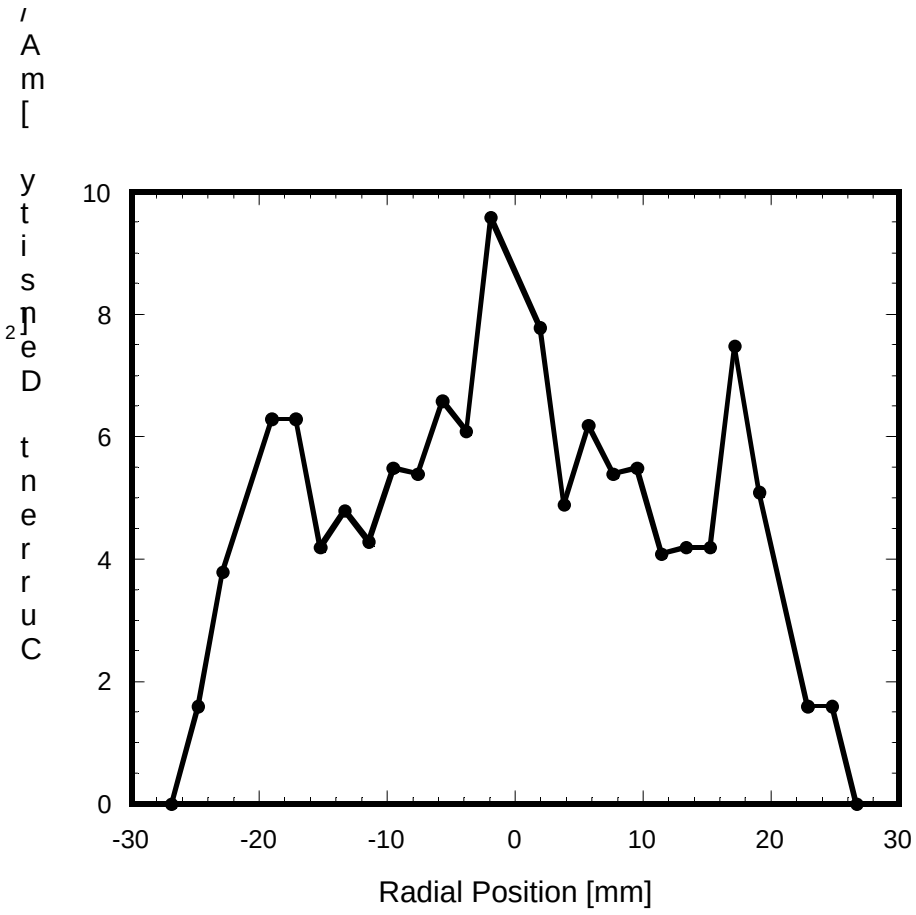
Current Density [A/m2]
10
8
6
4
2
0
-30
-20
-10
0
10
20
30
Radial Position [mm]

Figure 5.

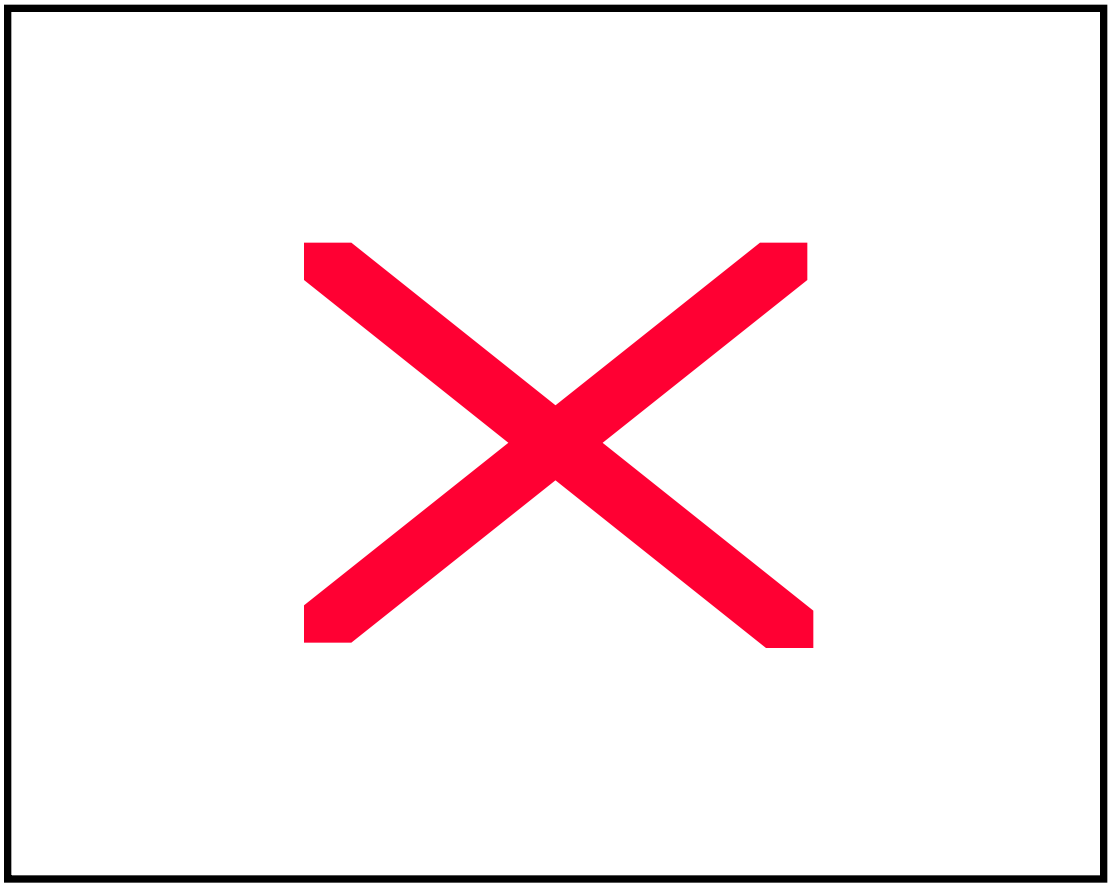

Figure 6.